Key role of organic carbon in the sunlight-enhanced atmospheric aging of soot by O_2

Chong Han, Yongchun Liu[1], Jinzhu Ma, and Hong He[1]

Research Center for Eco-Environmental Sciences, Chinese Academy of Sciences, Beijing 100085, China

Edited by Mark H. Thiemens, University of California at San Diego, La Jolla, CA, and approved November 19, 2012 (received for review July 24, 2012)

Soot particles are ubiquitous in the atmosphere and have important climatic and health effects. The aging processes of soot during long-range transport result in variability in its morphology, microstructure, and hygroscopic and optical properties, subsequently leading to the modification of soot's climatic and health effects. In the present study the aging process of soot by molecular O_2 under simulated sunlight irradiation is investigated. Organic carbon components on the surface of soot are found to play a key role in soot aging and are transformed into oxygen-containing organic species including quinones, ketones, aldehydes, lactones, and anhydrides. These oxygen-containing species may become adsorption centers of water and thus enhance the cloud condensation nuclei and ice nuclei activities of soot. Under irradiation of 25 mW·cm^{-2}, the apparent rate constants ($k_{1,obs}$) for loss or formation of species on soot aged by 20% O_2 were larger by factors of 1.5–3.5 than those on soot aged by 100 ppb O_3. Considering the abundance of O_2 in the troposphere and its higher photoreactivity rate, the photochemical oxidation by O_2 under sunlight irradiation should be a very important aging process for soot.

Soot, which originates from incomplete combustion, is a mixture of elemental carbon and organic carbon (OC) compounds (1, 2). It has been widely recognized that soot particles in the atmosphere are partly responsible for global climate change. For instance, the contribution of soot to global warming from the direct absorption of solar radiation is estimated to be second only to that of CO_2 (3). Soot also contributes to regional climate change and air quality; it has been associated with the increase in droughts or floods in China over the past 20 y (4, 5) and with haze formation over South Asia (6). Soot also poses a health risk by causing and enhancing respiratory, cardiovascular, and allergic diseases (7).

Once emitted into the atmosphere, soot undergoes aging processes through the uptake of reactive gases, such as OH, O_3, NO_2, NO_3, N_2O_5, HNO_3, and H_2SO_4 (8–17), and photochemical reactions (18). The aging processes of soot may not only affect the lifetime of some important gas-phase species, such as OH, O_3, and NO_3 (8–10, 14), but also modify the morphology, microstructure, and hygroscopic and optical properties of soot aggregates (19–22). At present, most studies have been focused on the kinetics of trace gas-phase species reactions with soot. Although large initial uptake coefficients for O_3 or NO_2 were measured in the dark, a rapid deactivation was usually observed because of the depletion of reactive sites (9, 11, 16, 23). Recently, it was found that UV light can persistently enhance the uptake reaction of NO_2 and O_3 on organic films or soot (24–28). This implies that photoreactions for soot may also be important in the troposphere. Compared with the uptake of gas-phase species by soot, however, the modification of soot during the aging processes remains unclear. A limited number of publications have studied changes of the surface composition and microstructure of soot during reaction with O_3, NO_2, and H_2SO_4 in the dark (2, 22, 29, 30). When soot was exposed to O_3 or NO_2, oxygen-related species or nitrogen-containing compounds were detected (2, 29, 30). Soot exposed to H_2SO_4 exhibited a marked change in morphology along with an increased fractal dimension and effective density (22). It should be pointed out that in all of these previous works, the aging processes focused only on the interactions between soot and gaseous pollutants in the dark. In this study, we investigated the aging process of soot resulting from photochemical oxidation by molecular O_2 and simulated sunlight. The photooxidation of surface OC is found to explain the aging process of soot.

Results and Discussion

Fig. 1 shows the infrared spectra of fresh fuel-rich flame soot as well as samples exposed to 20% O_2 in air for 12 h in the dark and under simulated sunlight irradiation. Little change was observed between the spectra of the fresh soot and that exposed to O_2 in the dark. On the other hand, as shown in Fig. S1, almost no changes were observed in the IR spectra for fuel-rich flame soot during irradiation by simulated sunlight in the high-purity N_2 atmosphere. However, the surface species changed dramatically when the fresh soot was exposed to O_2 and simulated sunlight (25 mW·cm^{-2}) for 12 h. The bands at 3,286 and 3,038 cm^{-1}, which were assigned to the stretching vibrations of alkyne C-H (≡C-H) and aromatic C-H (Ar-H) (30–33), respectively, decreased noticeably under irradiation. At the same time, a prominent increase in the intensities of the bands at 1,720, 1,591, and 1,241 cm^{-1} indicates the formation of several oxygen-containing species, such as carbonyl C=O and ether C-O (2, 30, 31, 34). These results definitely demonstrate that sunlight can significantly enhance the heterogeneous reactions of soot with O_2.

Fig. 2*A* shows the temporal changes of the IR spectra in the range of 1,800–1,500 cm^{-1} for the fuel-rich flame soot sample during photooxidation by O_2. The peaks at 1,591 and 1,628 cm^{-1} were related to carbonyl C=O conjugated to an aromatic ring (Ar-C=O), such as aromatic aldehyde, aromatic ketone, and aromatic quinone (2, 31, 32). The bands at 1,714 and 1,680 cm^{-1} originated from ketone and aldehyde C=O stretching, respectively (2). The peak around 1,734 and 1,772 cm^{-1} was assigned to C=O stretching of lactone or anhydride species (2, 32). The curve-fitting results are summarized in Fig. S2. Fig. 2*B* shows the dynamic changes of the integrated areas for bands at 1,772, 1,734, 1,714, 1,680, 1,628, and 1,591 cm^{-1}. The integrated areas of lactone or anhydride (1,772 and 1,734 cm^{-1}), ketone (1,714 cm^{-1}), aldehyde (1,680 cm^{-1}) and Ar-C=O (1,628 and 1,591 cm^{-1}) continuously grew with time as soot was exposed to O_2 and irradiated by simulated sunlight. These results demonstrate that oxygen-containing species can be formed in this reaction and their surface concentrations increase with aging time, leading to an increase in the O/C atomic ratio of soot.

It is well recognized that incomplete combustion can produce a broad range of organic compounds like saturated and unsaturated hydrocarbons, polycyclic aromatic hydrocarbons (PAHs),

Author contributions: C.H., Y.L., and H.H. designed research; C.H. performed research; J.M. contributed new reagents/analytic tools; C.H. analyzed data; and C.H., Y.L., and H.H. wrote the paper.

The authors declare no conflict of interest.

This article is a PNAS Direct Submission.

[1]To whom correspondence may be addressed. E-mail: ycliu@rcees.ac.cn or honghe@rcees.ac.cn.

This article contains supporting information online at www.pnas.org/lookup/suppl/doi:10.1073/pnas.1212690110/-/DCSupplemental.

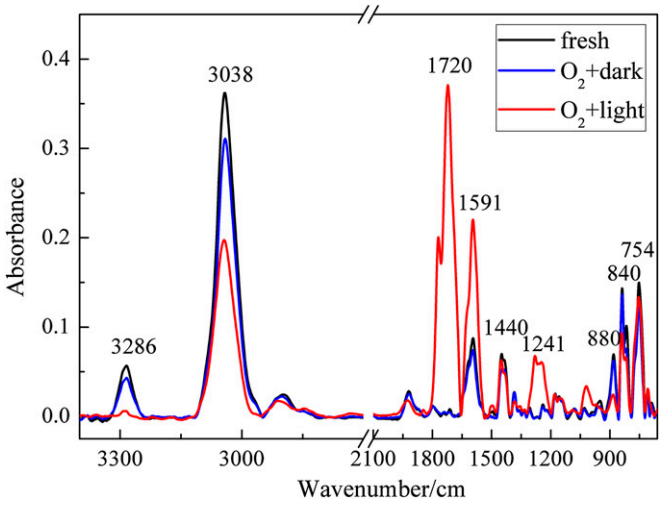

Fig. 1. ATR-IR spectra of fresh fuel-rich flame soot and samples exposed to 20% O_2 in air for 12 h in the dark and under simulated sunlight irradiation.

and partially oxidized organics (2, 13, 31, 35, 36). Adsorbed OC was also found on the surface of soot (2, 13, 21). According to the methods described by Daly et al. (2), the amount of condensed OC on the fuel-rich flame soot in this study was directly measured to be 6.0 wt % using thermal gravimetric analysis (TGA) (Fig. S3). To clarify the role of OC in the photochemical aging process of soot discussed above, the fuel-rich flame soot was preheated at 300 °C in nitrogen to remove the condensed OC. As shown in Fig. S4, the photochemical reactivity decreased drastically, as indicated by only slight changes in the spectra when the sample was exposed to O_2 under simulated sunlight irradiation. This suggests that OC was the main contributor to the photochemical aging process of soot by O_2. The dried fuel-rich flame soot residues after being extracted by *n*-hexane also showed a very low reactivity, as shown in Fig. 3*A*, in which only very weak peaks related to carbonyl C=O in the range of 1,800–1,500 cm^{-1} were observed during photochemical reaction. Fig. 3*B* illustrates the photochemical oxidation of the extracts mentioned above. Clearly, when exposed to O_2 and irradiated by simulated sunlight, the extracts gave the same products as those produced on the fresh fuel-rich flame soot under the same reaction conditions. Therefore, we can conclude that the photochemical aging of soot by O_2 results from the photochemical reaction of OC on the surface of soot particles.

The compositions of the *n*-hexane extracts were further identified using GC-MS. As shown in Fig. 4, the extracts mainly contain PAHs (such as anthracene, phenanthrene, fluoranthene, pyrene, and chrysene) and some unidentified components. The amount of PAHs with lower molecular weight, such as phenanthrene, anthracene, 4H-lyclopenta[def]phenanthrene, and 2-phenylnaphthalene, decreased after the oxidation of soot under irradiation (Fig. 4*A*), whereas little change for PAHs with higher molecular weight was observed under the same conditions (Fig. 4*B*). This suggests that PAHs with low molecular weight contributed the most to the photochemical aging of soot by O_2. Although aliphatic hydrocarbons were not detected using GC-MS, loss of the peak at 3,286 cm^{-1} in the IR spectra was observed, suggesting that aliphatic hydrocarbons can also take part

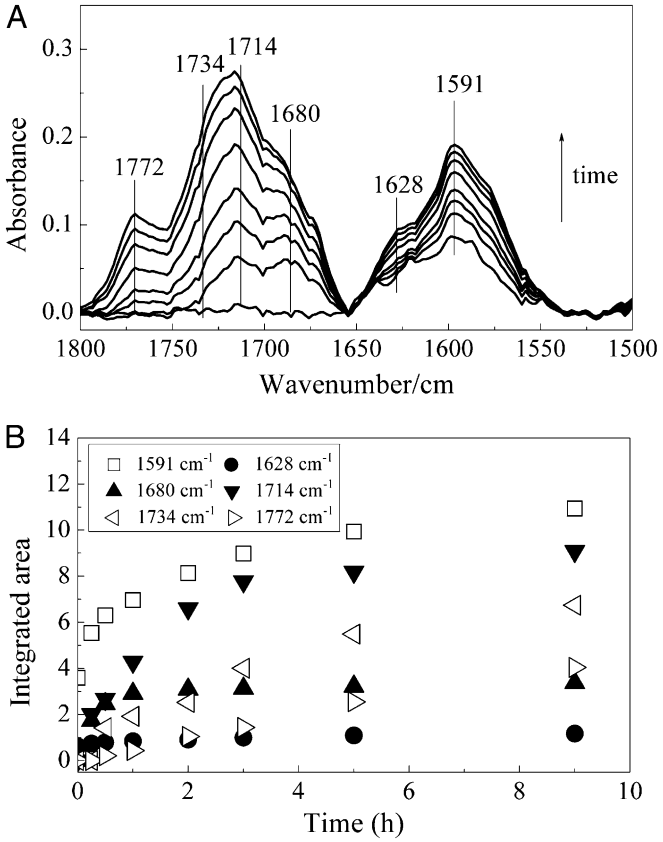

Fig. 2. (*A*) Temporal changes of in situ ATR-IR spectra in the range 1,800–1,500 cm^{-1} for the fuel-rich flame soot sample during photooxidation by 20% O_2. (*B*) Temporal changes in the integrated areas of peaks at 1,772, 1,734, 1,714, 1,680, 1,628, and 1,591 cm^{-1}.

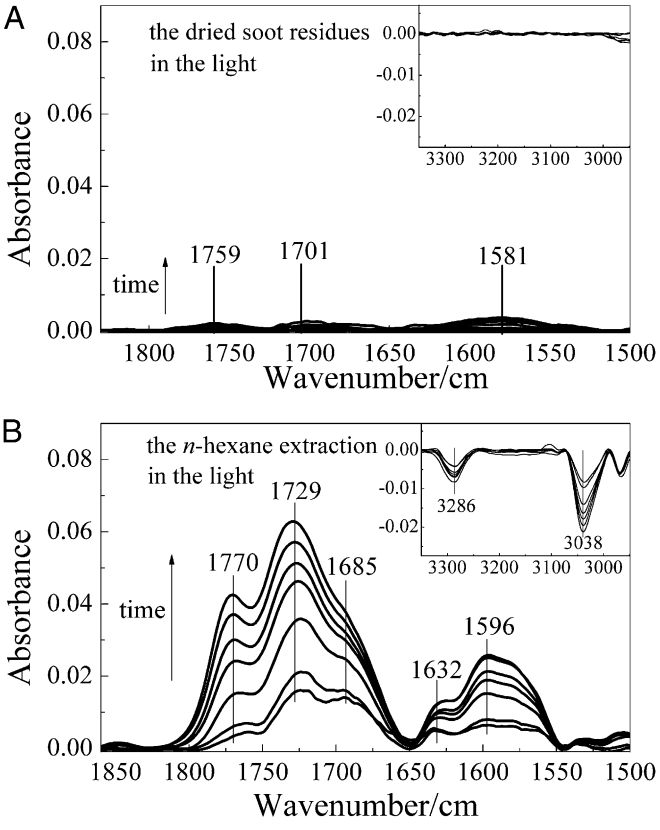

Fig. 3. Reactivity of the dried residues (*A*) and *n*-hexane extractants (*B*) of fuel-rich flame soot.

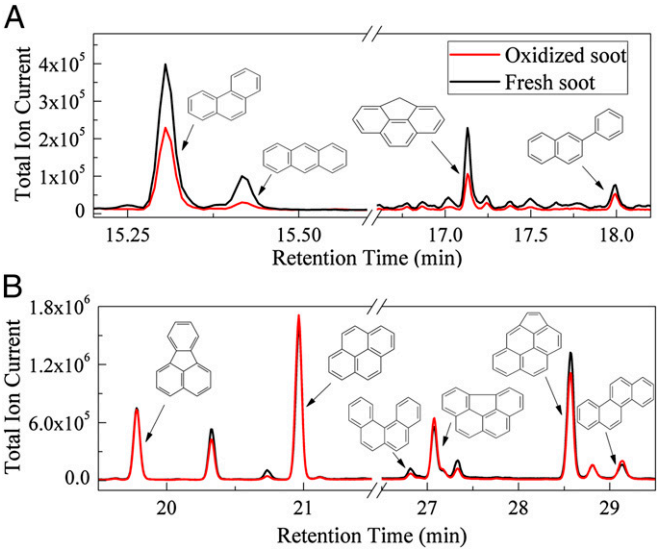

Fig. 4. Total ion chromatogram of the *n*-hexane extracts of fresh fuel-rich flame soot and that oxidized by 20% O_2 under simulated sunlight irradiation; (*A*) total ion chromatogram between 15.2 and 18.2 min of retention time; (*B*) total ion chromatogram between 19.5 and 29.5 min of retention time.

in the photochemical aging reaction of soot with O_2. The oxygenated and more polar compounds originating from the oxidation and combustion processes were not probed by GC-MS analysis. This may be ascribed to the method of obtaining OC by ultrasonic extraction using *n*-hexane, which should mainly extract nonpolar components. According to IR analysis, however, Fig. 2 clearly exhibits the formation of various oxygenated and more polar compounds, including aldehydes, ketones, quinones, lactones, and anhydrides, during the photochemical aging process of soot by O_2.

It is well recognized that PAHs can absorb sunlight in the visible (400–700 nm) and the UV regions (290–400 nm) of the solar spectrum due to their extensive π-orbital system (37). It has also been found that PAHs (anthracene, phenanthrene, fluoranthene, and pyrene) are good acceptors of singlet molecular oxygen, which can then react by an energy transfer mechanism followed by decomposition of thermally unstable peroxide products and formation of various aromatic aldehydes, acids, and quinones (37–41). Some PAHs, such as fluorene, are not good acceptors of singlet molecular oxygen but readily undergo photolysis at the solid–air interface by an electron transfer mechanism (42). Therefore, it can be postulated that the consumption of PAHs on soot should be related to these processes. Furthermore, oxygenated aromatic compounds such as anthraquinones and aromatic carbonyls, which are generated directly by combustion processes and upon PAHs oxidation, are well-known photosensitizers and thus induce the photodegradation of aliphatic hydrocarbons (43).

Combustion conditions, in particular the fuel/oxygen ratio, have an important influence on the composition and properties of soot (12, 24, 44). We also studied the effect of fuel/oxygen ratio on the photoreactivity of soot. Compared with fresh fuel-rich flame soot, fresh fuel-lean flame soot exhibited a stronger peak at 1,591 cm^{-1} for Ar-C=O and one weaker peak at 3,038 cm^{-1} for Ar-H (Fig. S5). The peak at 3,286 cm^{-1} related to alkyne (≡C-H) for fuel-lean flame soot disappeared. The integrated area ratio ($A_{Ar\text{-}C=O}/A_{Ar\text{-}H}$), which reflects the surface oxidation states of soot, increased from 0.36 to 1.10 when the fuel/oxygen ratio decreased from 0.18 to 0.10. Higher oxygen content in soot produced at lower fuel/oxygen ratio was also detected using elemental analysis by Stadler et al. (12). Fig. 5 shows the photochemical reaction results of the fuel-lean flame soot (the fuel/oxygen ratio was 0.10). However, only one new peak around 1,720 cm^{-1} was observed, whereas other peak intensities remained approximately unchanged under the reaction conditions. As discussed above, the photooxidation of soot by O_2 mainly produces oxygen-related functional groups. Thus it is reasonable to expect that the fuel-lean flame soot should exhibit a lower photochemical reactivity, because the sites with high photochemical reactivity on the sample surface should have been consumed during combustion. The consumption of reactive sites was supported by the higher $A_{Ar\text{-}C=O}/A_{Ar\text{-}H}$ for the fuel-lean flame soot. Additionally, the content of OC on fuel-lean flame soot was only 3.1 wt %, which is equivalent to half of that on the fuel-rich flame soot (Fig. S3). These results suggest that OC content and its oxidation state play a key role in the photochemical process of soot with O_2.

The evolution of the surface concentration of carbonyl compounds (Ar-C=O and C=O), aromatic compounds (Ar-H), and aliphatic hydrocarbons (≡C-H) on soot upon irradiation as a function of O_2 content was exponential in reaction time (Fig. S6), which suggests that the reactions are reasonably described by pseudofirst-order kinetics. Therefore, the experimental data were fit using a pseudofirst-order exponential function as shown in Eq. **1**,

$$ln\left(\left(A_t - A_p\right)/\left(A_0 - A_p\right)\right) = -k_{1,obs}t \qquad [1]$$

where A_t is the peak area at a given time t, A_0 is the initial peak area, A_p is the peak area at the plateau shown in Fig. S6, and $k_{1,obs}$ is the apparent rate constant of the pseudofirst-order reaction. Fig. S7 shows a linear correlation between the natural logarithm of peak area and irradiation time, confirming the first-order reaction nature of Ar-C=O, C=O, Ar-H, and ≡C-H species. By comparing their $k_{1,obs}$, it was evident that Ar-H and ≡C-H exhibited higher reaction rates, which were larger than that of carbonyl groups (Ar-C=O and C=O). This can be ascribed to the formation of other oxygen-containing species, such as ether (C-O, 1,241 cm^{-1}). For Ar-C=O, C=O, Ar-H, and ≡C-H, the correlation between their $k_{1,obs}$ and the O_2 concentration can be explained using the Langmuir-Hinshelwood mechanism (Fig. 6). Thus, the $k_{max}{}^{I}$ of Ar-C=O, C=O, Ar-H, and ≡C-H are 4.2×10^{-2}, 2.1×10^{-2}, 3.1×10^{-2}, and 3.8×10^{-2} min^{-1}, respectively.

As another important oxidant in the atmosphere, O_3 plays a significant role in atmospheric chemistry. To understand the relative importance of the photochemical aging of soot by O_2,

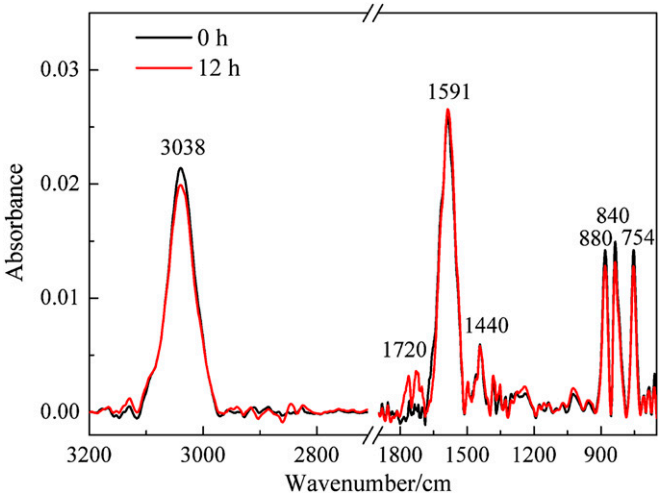

Fig. 5. ATR-IR spectra of fuel-lean flame soot exposed to 20% O_2 and simulated sunlight for 12 h.

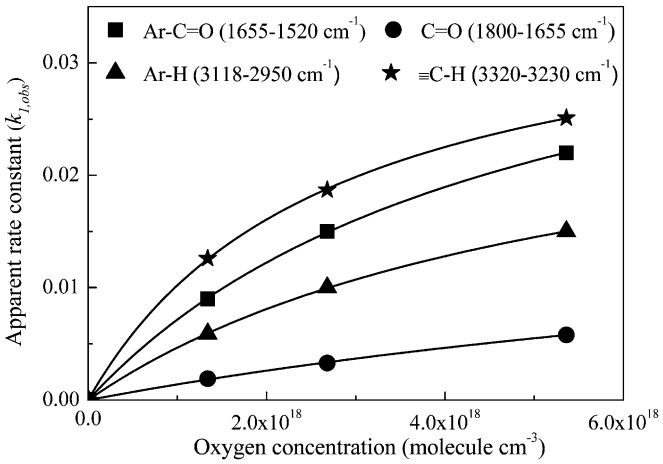

Fig. 6. Plot of apparent rate constant ($k_{1,obs}$) vs. oxygen molecule concentration.

heterogeneous reactions between fuel-rich flame soot and 100 ppb O_3 were also investigated in the dark and under irradiation. It was noticed that the products during aging of soot by 100 ppb O_3 were the same as those in the reaction of soot with 20% O_2 under irradiation (Fig. S8). As shown in Fig. 7 and Table 1, the $k_{1,obs}$ of Ar-C=O, C=O, Ar-H, and ≡C-H on soot aged by 20% O_2 was larger by factors of 3.0–5.0 than those on soot aged by 100 ppb O_3 in the dark, whereas it was larger by factors of 1.5–3.5 than those on soot aged by 100 ppb O_3 under irradiation of 25 mW·cm^{-2}. The average O_3 concentration in the atmosphere is 30 ppb (45), which is far less than that used in this study. On the other hand, it should be pointed out that previous studies have observed that O_3 led to much more vigorous oxidation of condensed phase, removing OC from soot by oxidation and volatilization (28, 46). However, little OC is lost from soot during the photo-aging by O_2 (*SI Materials and Methods, Loss of OC*). These results suggest that O_3 and O_2 affect the atmospherically relevant properties of soot differently. Under the light, O_3 should lead to more loss of OC and a more hydrophobic surface of aged soot, whereas O_2 leads to little loss of OC with an increase in the O/C atomic ratio and a more hydrophilic surface. Under atmospheric conditions, therefore, these are counteracting effects with different influences on atmospheric life and cloud condensation nuclei (CCN) activity of soot.

The sunlight-enhanced atmospheric aging of soot by O_2 may alter the atmospheric properties of soot, such as reactivity, CCN, or ice nuclei (IN) activity, optical properties, and photochemistry, as outlined below.

i) Reactivity: During the photochemical aging process by O_2, consumption of active components, including ≡C-H and Ar-H, can reduce the reactivity of soot toward the uptake of oxidizing gases such as OH, O_3, NO_2, NO_3, N_2O_5, and HNO_3 (8–16), thus affecting the tropospheric chemistry of these species.

ii) CCN or IN activity: As shown in Fig. 2, formation of various polar oxygen-containing species increases the hydrophilicity of soot (19, 47), which can enhance its ability to act as CCN or IN. It has been reported that elevated CCN levels can increase the cloud droplet concentration and updraft velocity but reduce the mean droplet size, leading to suppressed coalescence and warm rain but efficient mixed-phase precipitation (48).

iii) Optical properties and photochemistry: Soot also plays a significant role in radiative balance by strongly absorbing and scattering solar radiation at UV and visible wavelengths (49, 50), which are relevant to the photolysis rates of many oxidants (50, 51). Zhang and colleagues (50, 51) found that soot can reduce the photolysis frequencies of O_3 and NO_2 by absorbing sunlight, leading to a reduction in the concentration of HOx and O_3. However, the optical properties of soot greatly depend upon its morphology, composition, and structure (21, 22, 52, 53). Thus modification of soot during the photochemical aging process by O_2 may significantly alter its optical properties, resulting in changes in the effects of soot on the photochemistry of some atmospheric oxidants. As shown in Fig. S9, the oxidized soot exhibited larger absorbance than fresh soot in the range of 200–700 nm in UV-vis spectra. This may lead to more

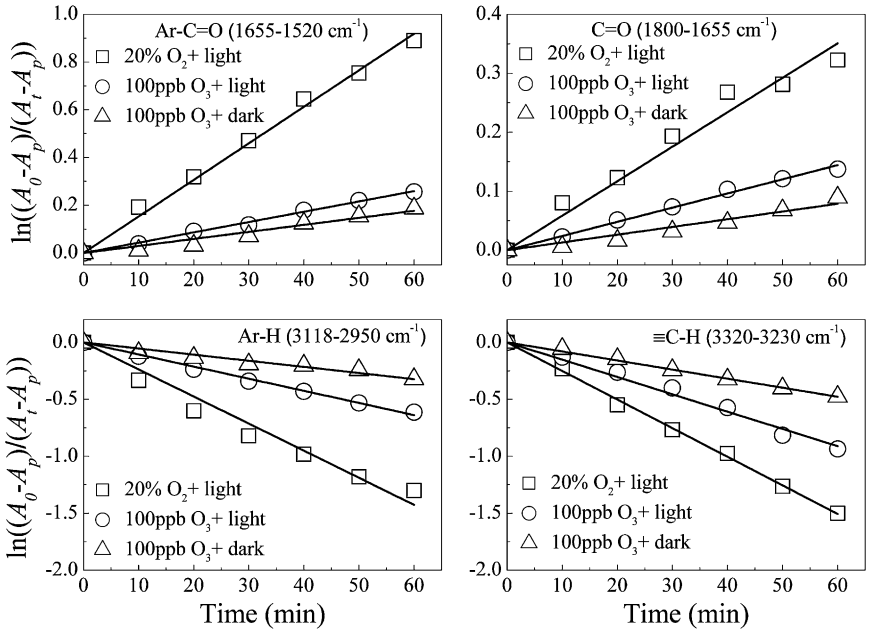

Fig. 7. Comparison of kinetics of Ar-C=O, C=O, Ar-H, and ≡C-H for oxidized fuel-rich flame soot (20% O_2) and ozonized fuel-rich flame soot (100 ppb O_3) in the dark and under simulated sunlight.

Table 1. Summaries of the $k_{1,obs}$ for Ar-C=O, C=O, Ar-H, and ≡C-H during the reaction of fuel-rich flame soot with O_2 and O_3

Conditions	$k_{1,obs}$ (Ar-C=O)	$k_{1,obs}$ (C=O)	$k_{1,obs}$ (Ar-H)	$k_{1,obs}$(≡C-H)
20% O_2 + light	1.5×10^{-2}	5.9×10^{-3}	2.4×10^{-2}	2.5×10^{-2}
100 ppb O_3 + light	4.3×10^{-3}	2.4×10^{-3}	1.1×10^{-2}	1.5×10^{-2}
100 ppb O_3 + dark	3.0×10^{-3}	1.3×10^{-3}	5.0×10^{-3}	8.0×10^{-3}

significant decreases in the photolysis rates of oxidants such as O_3 and NO_2. Certainly, the environmental and health effects of oxidized soot need to be further studied in the future.

Conclusions

Sunlight drastically enhances the aging process of soot by O_2, accompanied with the formation of oxygen-containing compounds, such as ketones, aldehydes, quinones, lactones, and anhydrides. Soot heated to 300 °C and dried soot residues extracted with *n*-hexane show low reactivity toward O_2, suggesting that the components active toward photooxidation should be OC rather than the carbon skeleton in soot. On the basis of IR spectra and GC-MS results, we can assume that photolysis of various PAHs with low molecular weight and aliphatic hydrocarbons contribute to the photochemical oxidation of soot. The fuel/oxygen ratio can significantly modify the reactivity of soot by influencing the OC content and degree of surface oxidation of soot. The functional groups Ar-C=O, C=O, Ar-H, and ≡C-H show pseudofirst-order reaction kinetics with O_2, and the relationship between their $k_{1,obs}$ and the O_2 concentration within 6.0×10^{18} molecule cm^{-3} follows the Langmuir-Hinshelwood mechanism. Under irradiation of 25 mW cm^{-2}, the $k_{1,obs}$ of Ar-C=O, C=O, Ar-H, and ≡C-H on soot aged by 20% O_2 was larger factors of 1.5–3.5 than that by 100 ppb O_3.

Materials and Methods

Soot Production. Soot particles were produced by burning *n*-hexane (AR, Sinopharm Chemical Reagent Co.) in a coflow diffusion burner. This coflow burner consisted of a diffusion flame that was maintained in an airflow, which was controlled by mass flow meters to regulate the fuel/oxygen ratio. The fuel was fed by a cotton wick extending into the liquid fuel reservoir. The airflow with a range of O_2 content from 21.5% to 32.5% was a mixture of high-purity oxygen and nitrogen. The combustion conditions were expressed as the molar ratio of the consumed fuel (measured by the mass of consumed *n*-hexane) to the introduced oxygen (obtained from the entrained airflow volume) during the combustion process. The fuel/oxygen ratio was in the range of 0.18–0.10. Thus, soot obtained at a fuel/oxygen ratio of 0.18 and 0.10 was relatively identified as "fuel-rich" flame soot and "fuel-lean" flame soot, respectively.

Photochemical Reaction. The in situ attenuated total internal reflection infrared (ATR-IR) spectra were recorded using a NEXUS 6700 (Thermo Nicolet Instrument Corp.) Fourier transform infrared (FT-IR) spectrometer equipped with a high-sensitivity mercury-cadmium-telluride (MCT) detector cooled by liquid N_2. Soot particles from the diffusion flame were directly deposited on the ZnSe crystal of the ATR-IR cell. The ATR-IR cell was sealed with quartz glass, through which soot was irradiated by a xenon lamp (500 W) having a continuous emission in the 350- to 700-nm range and a dominant wavelength at 480 nm. Light of the xenon lamp was transmitted by the optical fiber, which was located at 10 cm over the soot samples. Thus, total irradiance of light was 25 mW·cm^{-2} at the soot surface. During the irradiation the ozone concentration was lower than the detection limit (1.5 ppb) of the ozone monitor (Model 202, 2B Technologies). Before the reaction, soot was purged with 100 mL·min^{-1} N_2 at 298 K until the infrared spectrum was unchanged (*ca.* 1 h, shown in Fig. S1). Then, a mixture of high-purity oxygen and nitrogen was introduced into the ATR-IR cell. The spectra of soot were recorded (100 scans, 4-cm^{-1} resolution) using the blank ZnSe as reference. Infrared spectra remained unchanged when soot was irradiated for 12 h in high-purity N_2 (Fig. S1).

To examine the reactivity and composition of the organic fraction of soot, fresh fuel-rich flame soot was heated to 300 °C in nitrogen to evaporate OC without modifying the bulk elemental carbon (2). Soot particles after treatment were ultrasonically dispersed in H_2O and then deposited on the ZnSe crystal. The soot was purged with 100 mL·min^{-1} N_2 until the peaks of H_2O were not observed, and then a mixture of high-purity oxygen and nitrogen was introduced. In addition, ultrasonic extraction of fresh fuel-rich flame soot was performed in *n*-hexane, which has a low boiling point and shows no reactivity to O_2 under simulated sunlight. The extraction was performed for 10 min in the dark to avoid the oxidation of the organic components. Subsequently, oxidation of the extracts was examined in the ATR-IR cell after evaporation of the solvent. The reaction of the soot residues was also observed using in situ ATR-IR.

Methods. ***Thermal gravimetric analysis.*** The OC content of soot samples was investigated by thermal desorption using a commercial TG instrument (TGA/DSC1/HT1600, Mettler-Toledo). The amount of OC lost from the soot was recorded when the temperature was ramped from 30 to 300 °C at 10 °C·min^{-1} in nitrogen flow.

GC-MS analysis. The chemical composition of the extracts was also analyzed by GC-MS according to the following parameters: column HP 5MS (internal diameter 0.25 mm, length 30 m, film thickness 0.25 μm), injection volume 1 μL, inlet temperature 553 K, interface temperature 553 K, with the following temperature program: hold for 1 min at 333 K; increase temperature to 473 K at 10 K·min^{-1}; hold for 5 min at 473 K; increase temperature to 493 K at 5 K·min^{-1}; hold for 5 min at 493 K; increase temperature to 553 K at 5 K·min^{-1}; hold for 10 min at 553 K.

ACKNOWLEDGMENTS. We thank John Liggio for his instructive suggestions. This research was financially supported by the Strategic Priority Research Program of the Chinese Academy of Sciences (XDB05010300) and National Natural Science Foundation of China Grants 20907069, 50921064, and 20937004.

1. Muckenhuber H, Grothe H (2006) The heterogeneous reaction between soot and NO_2 at elevated temperature. *Carbon* 44:546–559.
2. Daly HM, Horn AB (2009) Heterogeneous chemistry of toluene, kerosene and diesel soots. *Phys Chem Chem Phys* 11(7):1069–1076.
3. Jacobson MZ (2001) Strong radiative heating due to the mixing state of black carbon in atmospheric aerosols. *Nature* 409(6821):695–697.
4. Chameides WL, Bergin M (2002) Soot takes center stage. *Science* 297(5590): 2214–2215.
5. Menon S, Hansen J, Nazarenko L, Luo Y (2002) Climate effects of black carbon aerosols in China and India. *Science* 297(5590):2250–2253.
6. Gustafsson Ö, et al. (2009) Brown clouds over South Asia: Biomass or fossil fuel combustion? *Science* 323(5913):495–498.
7. Sydbom A, et al. (2001) Health effects of diesel exhaust emissions. *Eur Respir J* 17(4): 733–746.
8. Bertram AK, Ivanov AV, Hunter M, Molina LT, Molina MJ (2001) The reaction probability of OH on organic surfaces of tropospheric interest. *J Phys Chem A* 105:9415–9421.
9. Lelièvre S, et al. (2004) Heterogeneous reaction of ozone with hydrocarbon flame soot. *Phys Chem Chem Phys* 6:1181–1191.
10. McCabe J, Abbatt JPD (2009) Heterogeneous loss of gas-phase ozone on n-hexane soot surfaces: Similar kinetics to loss on other chemically unsaturated solid surfaces. *J Phys Chem C* 113:2120–2127.
11. Arens F, Gutzwiller L, Baltensperger U, Gäggeler HW, Ammann M (2001) Heterogeneous reaction of NO_2 on diesel soot particles. *Environ Sci Technol* 35(11): 2191–2199.
12. Stadler D, Rossi MJ (2000) The reactivity of NO_2 and HONO on flame soot at ambient temperature: The influence of combustion conditions. *Phys Chem Chem Phys* 2: 5420–5429.
13. Khalizov AF, Cruz-Quinones M, Zhang R (2010) Heterogeneous reaction of $NO(_2)$ on fresh and coated soot surfaces. *J Phys Chem A* 114(28):7516–7524.
14. Saathoff H, et al. (2001) The loss of NO_2, HNO_3, NO_3/N_2O_5, and $HO_2/HOONO_2$ on soot aerosol: A chamber and modeling study. *Geophys Res Lett* 28:1957–1960.
15. Muñozy MSS, Rossi MJ (2002) Heterogeneous reactions of HNO_3 with flame soot generated under different combustion conditions. Reaction mechanism and kinetics. *Phys Chem Chem Phys* 4:5110–5118.
16. Kleffmann J, Wiesen P (2005) Heterogeneous conversion of NO_2 and NO on HNO_3 treated soot surfaces: atmospheric implications. *Atmos Chem Phys* 5:77–83.
17. Zhang D, Zhang R (2005) Laboratory investigation of heterogeneous interaction of sulfuric acid with soot. *Environ Sci Technol* 39(15):5722–5728.
18. Weitkamp EA, Sage AM, Pierce JR, Donahue NM, Robinson AL (2007) Organic aerosol formation from photochemical oxidation of diesel exhaust in a smog chamber. *Environ Sci Technol* 41(20):6969–6975.
19. Liu Y, Liu C, Ma J, Ma Q, He H (2010) Structural and hygroscopic changes of soot during heterogeneous reaction with $O(_3)$. *Phys Chem Chem Phys* 12(36):10896–10903.

20. Knauer M, et al. (2009) Soot structure and reactivity analysis by Raman microspectroscopy, temperature-programmed oxidation, and high-resolution transmission electron microscopy. *J Phys Chem A* 113(50):13871–13880.
21. Xue H, Khalizov AF, Wang L, Zheng J, Zhang R (2009) Effects of dicarboxylic acid coating on the optical properties of soot. *Phys Chem Chem Phys* 11(36):7869–7875.
22. Zhang R, et al. (2008) Variability in morphology, hygroscopicity, and optical properties of soot aerosols during atmospheric processing. *Proc Natl Acad Sci USA* 105(30): 10291–10296.
23. Aubin DG, Abbatt JPD (2007) Interaction of NO_2 with hydrocarbon soot: Focus on HONO yield, surface modification, and mechanism. *J Phys Chem A* 111(28):6263–6273.
24. Monge ME, et al. (2010) Light changes the atmospheric reactivity of soot. *Proc Natl Acad Sci USA* 107(15):6605–6609.
25. Stemmler K, Ammann M, Donders C, Kleffmann J, George C (2006) Photosensitized reduction of nitrogen dioxide on humic acid as a source of nitrous acid. *Nature* 440(7081):195–198.
26. Styler SA, Brigante M, D'Anna B, George C, Donaldson DJ (2009) Photoenhanced ozone loss on solid pyrene films. *Phys Chem Chem Phys* 11(36):7876–7884.
27. Jammoul A, Gligorovski S, George C, D'Anna B (2008) Photosensitized heterogeneous chemistry of ozone on organic films. *J Phys Chem A* 112(6):1268–1276.
28. Zelenay V, et al. (2011) Increased steady state uptake of ozone on soot due to UV/Vis radiation. *J Geophys Res* 116:D1103.
29. Al-Abadleh HA, Grassian VH (2000) Heterogeneous reaction of NO_2 on hexane soot: A Knudsen cell and FT-IR study. *J Phys Chem A* 104:11926–11933.
30. Kirchner U, Scheer V, Vogt R (2000) FTIR spectroscopic investigation of the mechanism and kinetics of the heterogeneous reactions of NO_2 and HNO_3 with soot. *J Phys Chem A* 104:8908–8915.
31. Cain JP, Gassman PL, Wang H, Laskin A (2010) Micro-FTIR study of soot chemical composition-evidence of aliphatic hydrocarbons on nascent soot surfaces. *Phys Chem Chem Phys* 12(20):5206–5218.
32. Akhter MS, Chughtai AR, Smith DM (1985) The structure of hexane soot I: Spectroscopic studies. *Appl Spectrosc* 39:143–153.
33. Cain JP, Camacho J, Phares DJ, Wang H, Laskin A (2011) Evidence of aliphatics in nascent soot particles in premixed ethylene flames. *Proc Combust Inst* 33:533–540.
34. Nieto-Gligorovski L, et al. (2008) Interactions of ozone with organic surface films in the presence of simulated sunlight: Impact on wettability of aerosols. *Phys Chem Chem Phys* 10(20):2964–2971.
35. Jonker MTO, Hawthorne SB, Koelmans AA (2005) Extremely slowly desorbing polycyclic aromatic hydrocarbons from soot and soot-like materials: evidence by supercritical fluid extraction. *Environ Sci Technol* 39(20):7889–7895.
36. Jonker MTO, Koelmans AA (2002) Sorption of polycyclic aromatic hydrocarbons and polychlorinated biphenyls to soot and soot-like materials in the aqueous environment: Mechanistic considerations. *Environ Sci Technol* 36(17):3725–3734.
37. Mallakin A, Dixon DG, Greenberg BM (2000) Pathway of anthracene modification under simulated solar radiation. *Chemosphere* 40(12):1435–1441.
38. Barbas JT, Sigman ME, Dabestani R (1996) Photochemical oxidation of phenanthrene sorbed on silica gel. *Environ Sci Technol* 30:1776–1780.
39. Springob C, Wolff T (1996) Photochemistry in porous materials IV: Oxygen quenching of the fluorescence of fluoranthenes absorbed on silica gel differing in pore size. *J Photoch Photobio A* 101:75–84.
40. Sigman ME, Schuler PF, Ghosh MM, Dabestani RT (1998) Mechanism of pyrene photochemical oxidation in aqueous and surfactant solutions. *Environ Sci Technol* 32: 3980–3985.
41. Barbas JT, Dabestani R, Sigman ME (1994) A mechanistic study of photodecomposition of acenaphthylene on a dry silica surface. *J Photoch Photobio A* 80: 103–111.
42. Barbas JT, Sigman ME, Arce R, Dabestani R (1997) Spectroscopy and photochemistry of fluorene at a silica gel/air interface. *J Photoch Photobio A* 109:229–236.
43. Vione D, et al. (2006) Photochemical reactions in the tropospheric aqueous phase and on particulate matter. *Chem Soc Rev* 35(5):441–453.
44. Chughtai AR, Kim JM, Smith DM (2002) The effect of air/fuel ratio on properties and reactivity of combustion soots. *J Atmos Chem* 43:21–43.
45. Logan JA (1985) Tropospheric ozone: Seasonal behavior, trends, and anthropogenic influence. *J Geophys Res* 90:10463–10482.
46. Smith DM, Chughtai AR (1997) Photochemical effects in the heterogeneous reaction of soot with ozone at low concentrations. *J Atmos Chem* 26:77–91.
47. Han C, Liu YC, Liu C, Ma JZ, He H (2012) Influence of combustion conditions on hydrophilic properties and microstructure of flame soot. *J Phys Chem A* 116(16): 4129–4136.
48. Zhang R, Li G, Fan J, Wu DL, Molina MJ (2007) Intensification of Pacific storm track linked to Asian pollution. *Proc Natl Acad Sci USA* 104(13):5295–5299.
49. Fan J, Zhang R, Tao WK, Mohr KI (2008) Effects of aerosol optical properties on deep convective clouds and radiative forcing. *J Geophys Res* 113:D08209.
50. Tie X, et al. (2005) Assessment of the global impact of aerosols on tropospheric oxidants. *J Geophys Res* 110:D03204.
51. Li G, Zhang R, Fan J (2005) Impacts of black carbon aerosol on photolysis and ozone. *J Geophys Res* 110:D23206.
52. Khalizov AF, Xue H, Wang L, Zheng J, Zhang R (2009) Enhanced light absorption and scattering by carbon soot aerosol internally mixed with sulfuric acid. *J Phys Chem A* 113(6):1066–1074.
53. Xue H, Khalizov AF, Wang L, Zheng J, Zhang R (2009) Effects of coating of dicarboxylic acids on the mass-mobility relationship of soot particles. *Environ Sci Technol* 43(8): 2787–2792.